Measuring noise in microwave metamaterials

M. C. K. Wiltshire, and R. R. A. Syms

Citation: Journal of Applied Physics **123**, 174901 (2018); doi: 10.1063/1.5018398
View online: https://doi.org/10.1063/1.5018398
View Table of Contents: http://aip.scitation.org/toc/jap/123/17
Published by the American Institute of Physics

Measuring noise in microwave metamaterials

M. C. K. Wiltshire[a] and R. R. A. Syms
Optical and Semiconductor Devices Group, Department of Electrical and Electronic Engineering, Imperial College London, Exhibition Road, London SW7 2AZ, United Kingdom

(Received 6 December 2017; accepted 12 April 2018; published online 1 May 2018)

Electromagnetic metamaterials are artificially constructed media composed of arrays of electrical circuits that can exhibit electric and magnetic characteristics unlike those of any conventional materials. However, the materials are lossy and hence noisy, so that the signal-to-noise ratio in practical situations is greatly reduced. In particular, operating in the double negative region, where both the permittivity and the permeability are negative so that the refractive index is real but negative, incurs significant loss and noise penalties. In this work, we report noise measurements on a double negative metamaterial at microwave frequencies and compare them with the results of a simple model based on a transmission line loaded with lossy elements that mimic the split ring resonators and fine wires of the metamaterial. A noise source is associated with the resistive part of each element, and these are added incoherently to predict the total noise spectrum of the metamaterial. The theoretical results are in good agreement with the measurements. In particular, we find that the measured noise spectrum has contributions from both electric and magnetic noise, but is dominated by the magnetic noise. This limits possible applications, even with optimised materials, to functions that cannot be realised by conventional means. *Published by AIP Publishing*. https://doi.org/10.1063/1.5018398

I. INTRODUCTION

Metamaterials[1,2] are artificial media that can be designed to provide electrical and magnetic properties outside the range normally encountered in nature. They consist of arrays of structures in which both the individual elements and the unit cell are small compared to the wavelength of operation; homogenization[3] of the structures then allows them to be described by the conventional electromagnetic (EM) constants of permittivity (ε) and permeability (μ), but with values that could not previously be obtained. For example, materials with simultaneously negative ε and μ can be built that have a negative refractive index,[4–6] and much attention has been given to the behaviour of such media[7] because they have the potential for sub-wavelength imaging.[8] Another concept enabled by metamaterials that has aroused substantial interest is cloaking,[9,10] in which any incident radiation is bent seamlessly around the cloaked object, thus rendering it invisible. Practical applications include their use in magnetic resonance imaging (MRI)[11–15] at radio-frequency (RF) and for steerable antennas[16,17] at microwave frequency.

In order to generate a magnetic response, and, in particular, a negative magnetic response, metamaterials generally rely on a resonant current circulating in a conducting structure, for example, the split-ring resonator (SRR)[2,18] which is widely used at microwave frequency. At lower frequencies, the Swiss Roll structure[2,19] has been investigated, although it has proved difficult to make in quantity, and resonant loop structures have been developed as magneto-inductive cables.[13,20,21] All these structures produce their magnetic response by virtue of resonant, circulating currents. Accordingly, there is some loss associated with them, and considerable effort has been made[6,22–24] to construct materials that are low loss. This is particularly important in practical systems, where the signal is usually at a premium. Furthermore, where there is loss, there is noise, and this has as great an impact on system performance as the loss itself: whereas loss can be overcome by amplification, noise cannot—it is amplified to the same extent as the signal.

Noise is endemic in all electrical systems. It arises from thermal fluctuations of the current carriers, and was first elucidated by Johnson[25] and Nyquist.[26] These authors showed that a resistor R at temperature T generates a noise voltage per unit bandwidth of

$$\langle V_n^2 \rangle = 4k_B TR, \tag{1}$$

where k_B is Boltzmann's constant. Some 25 years later, Callen and co-workers used statistical mechanics[27] and non-equilibrium thermodynamics[28] to generalise (1) into the Fluctuation-Dissipation Theorem (FDT).[29] This relates the fluctuations in a system with generalised coordinates X at temperature T, acted on by a generalised "force" F, to its generalised susceptibility χ, where $\chi = X/F$, through

$$\langle F^2 \rangle = 4k_B T\chi'', \tag{2}$$

where χ'' is the imaginary part of the susceptibility. Hence, the FDT links noise to loss. The fluctuations arise because when a "force" is applied at finite temperature, there is a continuum of states into which the system can move, whose probability of occupation is governed by Boltzmann statistics. Even when no "force" is applied, the system lies in a range of states, and can even move between these states when in thermal equilibrium. Thus, there are fluctuations in the system, which manifest themselves as noise.

[a]Email: michael.wiltshire@imperial.ac.uk

Can we apply this to a practical system, for example, a sample of metamaterial? In principle, the FDT tells us how much noise will be generated, but it says nothing about the impact of the nature and the size of the sample on the noise: this detail must all be contained in the susceptibility.[30] The core of this problem was tackled by Rytov,[31] who included noise sources (determined by the FDT) in the Maxwell curl equations. The solutions were expressed as Green's functions, which propagate through the medium as spherical waves, and are then integrated incoherently to obtain the resulting noise. However, although this formalism is rigorous, it is not easily used for treating practical problems. In the long wavelength, low frequency limit, it is analogous to calculating the demagnetising factor[32] for an arbitrary shaped sample; when retardation is taken into account, the problem is even less tractable.

An alternative approach has been developed by one of us and co-workers.[33,34] This is based on a finite, one-dimensional transmission-line model which permits the integration in Rytov's theory to be replaced by a summation, thus rendering the problem computable. In this approach, we recognise that each element has a finite resistance and associate a noise voltage with that resistance; if the resistive element is in a resonant circuit, the noise spectrum will also be resonant.[35] Since we have an array of such resistors, they will all generate a noise voltage and these must be added incoherently to obtain the total noise. Furthermore, if the resonant loops are coupled, so that there is a spectrum of magneto-inductive[36] or electro-inductive[37] waves, the noise spectrum is also modified. Thus, in metamaterials, where we rely on resonances and coupling to provide the exotic responses in the frequency range that we wish to exploit, the noise spectrum will be concentrated in just those same regions. The magneto- and electro-inductive waves couple with the electromagnetic waves that also propagate through the medium. The strength of this coupling determines how much of the internal noise actually appears in the outside world; the rest is trapped in the medium.

In a previous paper,[38] we investigated the trapped noise in an RF metamaterial by using a near-field probe to couple directly to the noise waves in the sample. We described the sample using the circuit model above and found good agreement between the measured and modelled noise spectra. In a second paper,[39] also working at RF, we explored the noise characteristics of magneto-inductive cables. There, the noise was generated inside the cable by the resonant elements as in Ref. 38, but was only observed when it left the cable. Again, we modelled the system using the circuit approach above and obtained good agreement between the measured and calculated noise spectra.

Here, we turn our attention to the microwave region, where the majority of metamaterials function and, in particular, we consider a so-called double negative or negative index material. This has both a negative permittivity and a negative permeability, but a finite transmission by virtue of the real part of its (negative) refractive index. It is constructed by combining a dielectric metamaterial with a magnetic one and matching their characteristics to provide the desired response.[7,40,41] Then, both subsystems will contribute to the noise, i.e. there is both electrical noise and magnetic noise in contrast to the more common case when electrical noise alone is considered. Our approach is as follows. In Sec. II, we first describe the construction and characterisation of the sample and then proceed to the noise measurements and their analysis. In Sec. III, we model the system using the one-dimensional circuit model described above and compare the calculated and measured data. We discuss the limitations and implications of our results in Sec. IV and draw our conclusions in Sec. V.

II. EXPERIMENTAL MEASUREMENTS

The noise measurements were made with the metamaterial samples placed inside a waveguide, so that a one-dimensional approach could be adopted. This allowed us to adopt the same procedure as in our previous work[39] and simplified the sample design by only requiring planar arrays of elements rather than a three-dimensional geometry.

A. Metamaterial design and characterisation

Our equipment (Agilent N1996A Spectrum Analyser) limited us to an upper frequency of 6 GHz, so a metamaterial that had a negative index region around 4.5 GHz would be ideal. Furthermore, a close-packed material was needed to maximise the noise signal in the active region. We had available as the magnetic metamaterial the original SRR structure made by the Marconi group in 1999, Fig. 1(a). This consisted of pairs of concentric split rings, each ring being 0.5 mm wide with a 0.5 mm gap in it, with the rings separated by 0.1 mm. The outer diameter was 5 mm and the rings were distributed on a square grid with a unit cell of 5.5 mm. They were fabricated on 25 mm wide strips of printed circuit board (PCB) with 1 oz (36 μm) copper on 1.6 mm FR4. This is a close-packed structure and FR4 is a lossy substrate. Additional losses arise from the finite conductivity of copper, rising with the frequency due to the skin effect. The overall material, therefore, has high loss, and hence is noisy. It has a resonance in its permeability at about 4.5 GHz, above which the material has negative permeability. To match this material, we designed a "fine-wire" dielectric metamaterial [Fig. 1(b)], which consisted of narrow (0.5 mm) copper tracks etched on a printed circuit board (see, e.g., Ref. 42), with a unit cell to

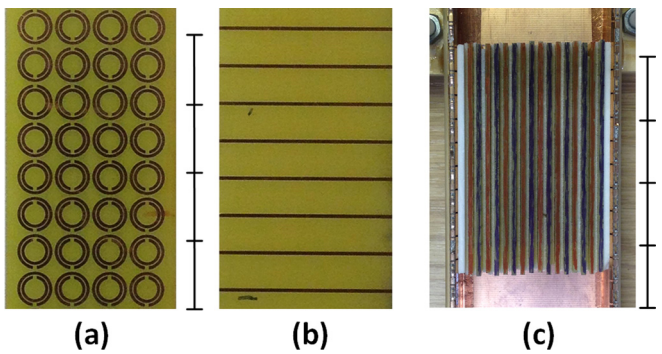

FIG. 1. (a) SRR and (b) wire components used to construct the metamaterial; the scale has 10 mm divisions. (c) shows the 12-unit cell CMM material, with alternate layers of SRRs (red) and "wires" (blue) spaced by Rohacell sheets, mounted in the waveguide; the scale has 20 mm divisions.

match that of the magnetic material and a sample width slightly greater than the 25 mm of the split-ring samples, to ensure that contact was made to the waveguide walls, so that the wires could be treated as being continuous rather than cut. These elements were assembled into slabs composed of strips of SRRs, wires, or alternating sheets of SRRs and wires to provide a combined metamaterial (CMM). The layers were separated by Rohacell® foam sheets (4 mm thick for the SRRs or wires alone, 1 mm for the combined medium), so that the unit cell dimension was preserved in all three directions, with the slabs being 8 unit cells wide and 4 unit cells high. Provided that there is an integral number of unit cells symmetrically placed in a symmetric waveguide, the transverse order of stacking (i.e., SRR–"wires"–SRR–"wires" or "wires"–SRR–"wires"–SRR) is unimportant. Samples were prepared with 4, 6, 8, and 12 unit cells in the propagation direction and mounted within the guide [see Fig. 1(c)].

To accommodate these slabs, a demountable custom waveguide was constructed, of height 25 mm and width 50 mm, whose usable frequency range was 3–6 GHz, thus bracketing the 4.5 GHz resonance frequency of the ring structure. No demountable waveguide with these dimensions was commercially available. The waveguide was constructed from an un-patterned PCB (FR4 with 36 μm copper), and was 945 mm long. The lid was held in place by seven equally spaced clamps, and good contact was ensured by using beryllium-copper sprung finger stock between the body and the lid. The waveguide was fed near its closed end by a monopole transmitter probe, with a similar receiver probe placed 830 mm from the transmitter probe, with the waveguide being terminated by an absorbing plug. This consisted of a stack of resistive foam, with the first few layers having holes cut in them to provide an absorption gradient and hence reduce reflections. The objective of this asymmetric structure was to reduce the effect of standing waves in the waveguide.

As a preliminary check on the performance of our materials, we modelled their behaviour using the commercial electromagnetic simulation software HFSS (ANSYS, Canonsburg, PA). First, a single unit cell of the SRR structure with periodic boundary conditions was modelled; this showed that the SRR had a resonant frequency of 4.35 GHz, whereas the identical ring structure, but without splits in the rings (denoted CRR), had no resonance in the frequency range of interest. Adding rings to the sample broadened and deepened the resonance as expected. Modelling the wire structure showed that the plasma frequency was predicted to be 11.8 GHz, and that the permittivity was negative at lower frequencies. We also modelled a CMM sample, because it is well known that there is an interplay between the rings and the wires in such samples that leads to a reduction in the plasma frequency.[43] In the present case, we found the effective plasma frequency for the CMM to be 7.2 GHz, significantly lower than that for the "wires" alone.

These predictions were confirmed by direct measurements using an Agilent E5071B vector network analyser (VNA). The resonant frequency of a single SRR was measured to be 4.6 GHz using a pair of small loop probes disposed on either side of the sample. This is a little higher than modelled, but is consistent with our other measurements (see later) and probably arises because the gap between the rings is slightly larger than the 0.5 mm used in the models. The effective plasma frequency of the "fine-wire" material was measured in a waveguide, using a Rohde & Schwarz ZVA67 VNA (courtesy of Professor Norbert Klein), and was found to be ~12.5 GHz. Again, this is a little higher than modelled, but is probably due to the "wires" being slightly thicker or wider than modelled. We also made measurements on a CMM sample, finding an effective plasma frequency for the CMM of 8.5 GHz, consistent with the modelled result.

Ideally, we would extract the full details of the permittivity and the permeability of the samples from measurements of the *S*-parameters in the waveguide (see, e.g., Refs. 44–46), so that they can be used in the noise modelling. However, it is well known that very accurate calibration is necessary to provide reliable results, and the sample needs to fill the guide, with no gaps around the edges. Neither was possible here: a full TRL (through–reflection–line) calibration[47,48] was attempted but was not sufficiently accurate to be stable and, by their very nature, the samples did not totally fill the guide. Therefore, it was not possible to perform the conventional extraction procedure in this work. Instead, we calibrated our VNA with open, short, load terminations in place of the waveguide ports and just measured the transmission, S_{21}.

There were significant "ripples" on all the measured spectra because of imperfect matching between the feed cables and the waveguide probes. It has not been possible to deembed the samples and hence remove these ripples using calibration spectra. Furthermore, there are reflections from both faces of the sample that can give rise to standing waves in the waveguide, and hence additional "ripples" in the spectrum whose period depends on the position of the sample. To minimise the impact of these, we used the longest possible distance between the probes (830 mm) and placed the sample close (within 10 mm) to the transmitter probe. Then, the period of interference between the sample input face and the transmitter probe becomes very long, whereas that between the exit face and the receiver probe is approximately the same as that for the empty guide. Numerical filtering was then used to eliminate these interferences from the spectra. The resulting transmission spectra are shown in Fig. 2(a)–2(c).

The empty waveguide has an average transmission of −5.5 dB; this is due to the demountable construction and the imperfect matching of the feed and receiver probes to the waveguide itself. The spectra of the wires show strong attenuation, −50 to −60 dB, consistent with the permittivity being negative below the effective plasma frequency. The SRR samples transmit above and below the resonance in the permeability: this is centred at 4.5 GHz and broadened by coupling between the elements both within individual strips and between strips. Furthermore, the stop band has a shallower cut-off towards a high frequency, consistent with the permeability becoming negative above the resonant frequency. Finally, the CMM spectra show a transmission peak in the region where the SRR and wires have negative permeability and permittivity, respectively, thus indicating that this is potentially a region of negative real refractive index.

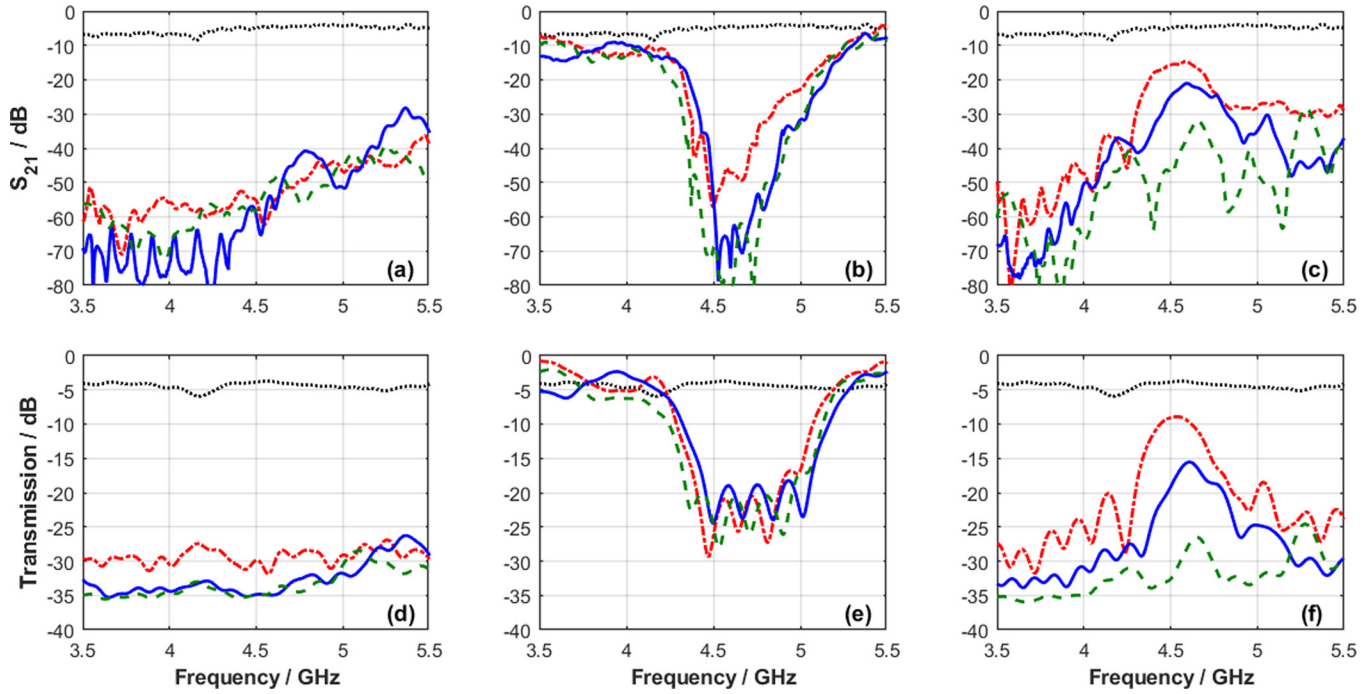

FIG. 2. Directly measured S_{21} spectra (a)–(c), and transmission spectra derived from noise data (d)–(f) for the empty waveguide (black dotted lines) and (a) and (d) wire, (b) and (e) ring, and (c) and (f) combined samples for 4-cell (red chain lines), 6-cell (blue full lines), and 8-cell (green dashed lines) metamaterial samples.

However, the presence of a transmission peak in a CMM where the SRRs alone had a stop-band is not conclusive proof that the CMM has a negative index in that region.[43] There are two factors that must be taken into account in addition to the simple superposition model: first, the SRRs have an electric response of their own, and accordingly shift the effective plasma frequency downwards; second, the currents in the wires interact with those in the SRR to move the magnetic resonance of the latter to higher frequency. Thus, it is possible that the peak observed in the CMM is actually a positive index peak. Furthermore, the SRRs in the present work are not symmetric with respect to the electric field: the gaps are oriented along OZ, the propagation direction, rather than along OY, the vertical, electric field direction. Therefore, some magneto-electric effects are also possible. To resolve these concerns, a set of samples was made with only 4 unit cells in the propagation direction, so that they could be rotated in the waveguide to align the gaps in a vertical direction. In addition, a second set of such samples was made with closed gaps (closed ring resonators or CRRs[40]), that had an electric response comparable to the SRRs, but no magnetic response, and transmission measurements were made as before.

First, we verified that the CRR and empty guide spectra were very similar, showing that the CRRs did not attenuate the signal. We also noted that the spectrum of the wires alone showed uniform attenuation across the entire frequency range with no evidence of cut-wire characteristics. The SRRs with gaps aligned along the propagation direction (OZ) had a stronger response than those with their gaps along the electric field direction (OX) because there is magneto-electric coupling in the OZ orientation, through which both the electric and magnetic fields can induce a magnetic resonance response. In OX orientation, the electric field cannot interact with the magnetic response. We then combined the wires with the SRR or CRR components with the wires arranged symmetrically between the layers of the SRRs, thus minimising their coupling to the SRRs. Both orientations of the SRRs showed a weak transmission at about 4.6 GHz, whereas the CRR + wire combination showed no difference from the bare wire spectrum. Accordingly, we can rule out both the shifting of the effective plasma edge to below, and also the shifting of the effective magnetic resonance to above our frequency region of interest, thus confirming that the CMM peak at 4.6 GHz is due to a region of negative refractive index.

B. Noise measurements

The conventional method for measuring the noise figure (NF) is to use a switchable noise source and a noise figure analyser. If the noise source generates a noise power N_0 when off and $N_H = \alpha N_0$ when on, and the ratio Y of the noise powers is measured, then the noise factor, F, and hence the noise figure, NF, which are defined as

$$F = SNR_{in}/SNR_{out} \quad \text{and} \quad NF = 10\log_{10}(F) \tag{3}$$

can be determined as

$$F = \frac{\alpha - 1}{Y - 1} = \frac{ENR}{Y - 1}, \tag{4}$$

where $ENR = \alpha - 1$ is the excess noise ratio of the switchable noise source. For a sequence of N devices, with noise factors $F_1, F_2, \ldots, F_N$ and gains $G_1, G_2, \ldots, G_N$, the total gain is $G = G_1 \cdot G_2 \cdots G_N$ and the total noise factor is[49]

$$F = F_1 + \frac{F_2 - 1}{G_1} + \frac{F_3 - 1}{G_1 G_2} + \cdots + \frac{F_N - 1}{G_1 G_2 \cdots G_{N-1}}. \quad (5)$$

By measuring the gain and the noise factor of the system as it is built up, the noise factor of each element can be extracted in turn.

Rather than just obtaining the ratio Y, we have preferred to measure the noise spectra individually, as in our previous work,[38,39] so that the gain and the noise power, as well as the noise factor, can be determined for each component. Accordingly, we used an Agilent N1996A Spectrum Analyser (SA) to record spectra at 1001 points in the frequency range 2.5–6.0 GHz, with a resolution bandwidth of 5 MHz and a video bandwidth of 100 Hz. The noise was generated by a switchable noise generator (BBGEN[50]), which was switched on and off for alternate scans. Its ENR in the frequency range of interest is approximately 17.5 dB when used with a 6 dB attenuator. The signal at the waveguide output was amplified using a CA08–4011 pre-amplifier[51] before being routed to the SA. Typically, 512 scans of each state were accumulated and their rms average taken. We made four sets of measurements, each of two spectra, one with the noise source switched on and the other one off. We recorded the noise powers observed for the SA alone, for the pre-amplifier + SA, for the empty waveguide + pre-amp + SA, and finally when the metamaterial sample was placed in the waveguide. It is then straightforward to find the gain (or transmission) of the sample and its noise power spectrum. The transmission spectra are shown in Figs. 2(d)–2(f) and are very similar to the directly measured S_{21} spectra, but do not reach such low transmission values because of the noise floor in these measurements is not as low as that for the VNA.

We see that the wire samples have very low transmission, as expected for a material with a negative permittivity, with the 4-cell sample having marginally higher transmission that the other two samples. The SRR samples show a strong dip in transmission at 4.5–4.8 GHz, consistent with a negative permeability region above the resonance frequency. Finally, the CMM shows an increase in transmission in the same region as the SRRs showed a dip, indicating the presence of a (lossy) region of real negative index. The transmission falls with increasing sample length, as expected.

Figures 3(a)–3(c) show the noise power spectra derived from these data. We see that the noise from the wires increases towards low frequencies, and flattens off below about 4.2 GHz; all three samples give similar spectra. The SRR samples show a broad maximum in their noise spectra corresponding to the dip in their transmission spectra. The CMM spectra are similar to those for the wires, but with a larger intensity where the SRRs show their peak power.

Finally, we combine the noise power with the transmission to obtain the Noise Figure (NF); this is shown in Figs. 3(d)–3(f). Once again, both the wire and the SRR spectra show saturation at their minimum transmission (or maximum NF). However, the CMM spectra show a minimum in the noise figure at the transmission peak, with a lowest NF of 9 dB for the 4-cell sample at 4.54 GHz; this is increased and shifted to higher frequency for the longer samples. Also shown is the NF for the empty waveguide; this takes into account not only the losses and noise in the guide itself, but

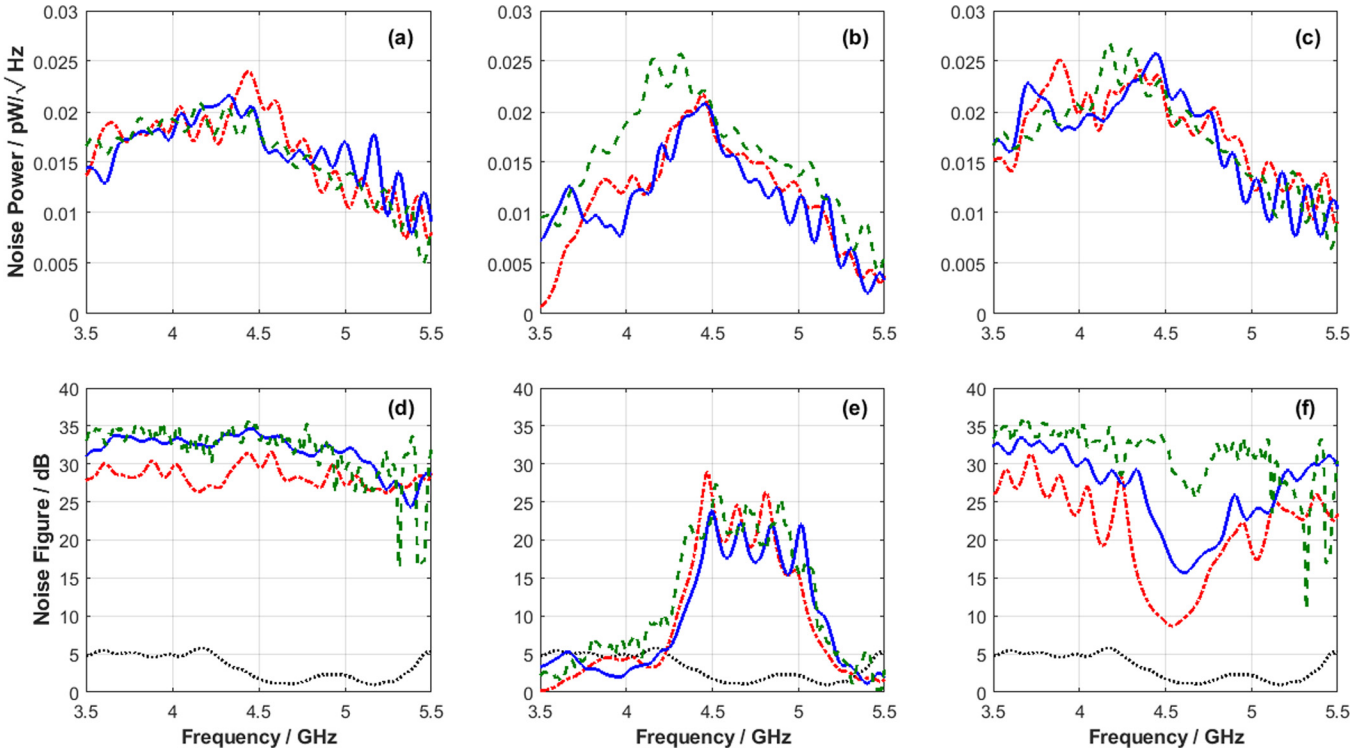

FIG. 3. (a)–(c) Noise power $\left(pW/\sqrt{Hz}\right)$ and (d)–(f) noise figure (dB) for (a) and (d) the wire, (b) and (e) the SRR, and (c) and (f) the CMM metamaterial samples with 4-cells (red chain lines), 6-cells (blue full lines), and 8-cells (green dashed lines). The noise figure of the metamaterial samples is compared to that of the empty waveguide (black dotted lines).

also any extra noise generated by the absorbing plug in the open end as described above.

III. CALCULATION

There are, in principle, two ways to calculate the noise from a specific sample; we may think of them as macroscopic and microscopic approaches. In the macroscopic approach, we invoke the Fluctuation Dissipation Theorem (FDT)[27–29] and relate the noise power to the imaginary part of the susceptibility. In the microscopic approach, which we use here, we develop circuit models for the individual components, the SRRs, the wires, and the waveguide. We attribute uncorrelated noise sources to each of the lossy elements and then apply circuit theory to calculate the overall noise output.[33,34]

We model the material as a transmission line and replace the elements within the unit cell by their circuit equivalents. We represent the electromagnetic (EM) wave travelling through the metamaterial by means of a lossless transmission line [see Fig. 4(a)], with series inductance $L_0 = \mu_0 a$ and shunt capacitance $C_0 = \varepsilon_0 a$ in each section of length a, where μ_0 and ε_0 are the permeability and the permittivity, respectively, of free space. The SRRs are described as resonant circuits with inductance L_R and capacitance C_R, which are inductively coupled via a mutual inductance M_R to the EM-wave line, and are also coupled inductively via the mutual inductance M to their neighbours. The fine wires are described by introducing shunt inductors, L_W, into the transmission line. A finite slab of thickness d of this material surrounded by free space can be modelled as a set of $N = d/a$ sections terminated by loads $Z_0 = \sqrt{\mu_0/\varepsilon_0}$, as shown in Fig. 4(a). Propagation of an electromagnetic wave can then be modelled by introducing a signal source at one end and calculating the transmitted and reflected powers.

The noise in this system is modelled by associating with each lossy element a series voltage source of magnitude equal to the Johnson noise generated by the resistive component. Thus, both the SRRs and the wires have losses associated with their inductive components.

Syms *et al.*[33] have shown that the parameters in this circuit can be related to the effective permittivity and permeability of the metamaterial, formulating an effective abstraction of the circuit [see Fig. 4(b)] by including a frequency dependent capacitance which represents the permittivity and a frequency dependent inductance which represents the effective permeability. These have the well-known effective medium forms

$$\varepsilon(\omega) = 1 - \frac{\omega_p^2}{\omega(\omega + i\gamma_e)} \tag{6}$$

and

$$\mu(\omega) = 1 - \frac{F}{1 + \kappa - \omega_0^2/\omega^2 + i\omega_0/\omega Q_0}. \tag{7}$$

In (6), γ_e is the collision damping frequency for the wires whose plasma frequency is ω_p. In (7), ω_0 is the resonant frequency of the SRR, which is determined by L_R and C_R, and Q_0 is its quality factor, related to the damping factor, $\gamma_m = \omega_0/Q_0$; F is the filling factor, related to the coupling factor M_R, and $\kappa = 2M/L_R$ is the inter-ring coupling parameter. The noise associated with the inductances is represented by voltage sources V_R which describe the magnetic noise and current sources I_W which represent the electrical noise. In a bandwidth df, these are given as

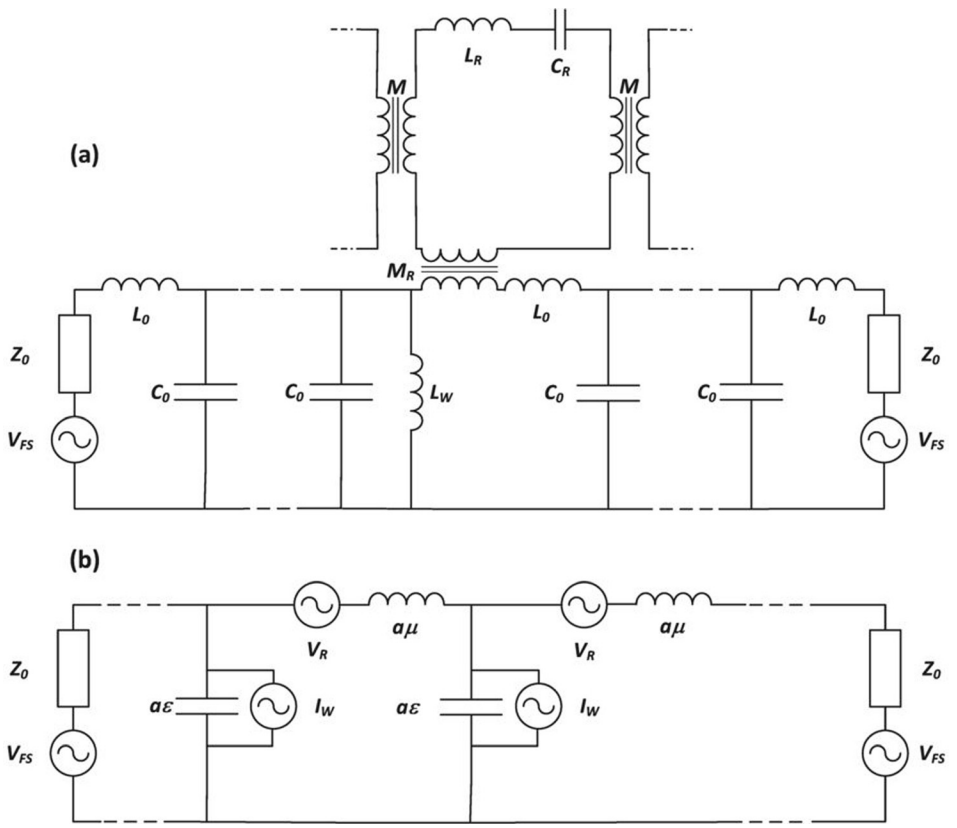

FIG. 4. (a) Transmission line circuit model of a metamaterial. Free space is represented by the L_0, C_0 line, terminated by Z_0; the wires contribute a shunt inductance L_W, and the rings are represented by L_R, C_R, and are mutually coupled by M, and coupled to the line by M_R. Each lossy component contributes a noise voltage (not shown). (b) After abstraction, the noise in each unit cell is represented by V_R and I_W for the rings and wires, respectively; the rings contribute to the effective permeability, μ, whereas the wires contribute to the effective permittivity, ε.

$$V_R V_R^* = 4k_B T\mu_0\mu'' adf \quad \text{and} \quad I_W I_W^* = 4k_B T\varepsilon_0\varepsilon'' adf, \quad (8)$$

respectively. Here, μ'' and ε'' represent the imaginary parts of the relative permeability and permittivity, respectively.

We can now use this transmission line model to calculate the noise performance of the metamaterial. We write down Kirchhoff's equations for the system, which are now in a matrix form, and solve them for the contribution from each unit cell to the output noise. There are two branches of the solution: one describes magneto-inductive waves whose associated noise is trapped in the metamaterial[38] and the other the electromagnetic wave which we study here. The individual contributions are summed incoherently to provide the total output noise.

We now consider the values of parameters in (6) and (7). From the measurements of the plasma frequencies, we know ω_p in both the pure wire (12.5 GHz) and the CMM (8.5 GHz) samples, so we only need an estimate of γ_e. Accordingly, we ran a series of calculations for the pure wire system, varying γ_e, and compared the frequency dependence of S_{21} with the measured result. The best match occurred for $\gamma_e = 0.15$, which is quite a high value, but is consistent with what is expected at this frequency for copper tracks etched on a standard circuit board.

From the measurements on a single SRR, we obtain $\omega_0 = 4.68$ GHz and $Q_0 = 35$, so we require estimates of F and κ. To obtain these, we ran a series of calculations for the ring sample, varying each parameter, in turn: κ alters the peak frequency of the SRR sample, whereas F affects the shape of the S_{21} response and also shifts the frequency of the noise peak. By matching the S_{21} spectra, we find $\kappa = 0.05$ to give the best result, and using both the S_{21} and noise results, we find $F = 0.23$.

As noted above, the CMM has a different value of ω_p from the pure wire material: this arises because there is coupling between the wires and the SRRs which acts to lower the effective plasma frequency of the wires. This coupling also acts on the SRRs themselves, shifting their resonance frequency in the CMM environment. We, therefore, expect to find that a different value of κ is required to describe the CMM spectra, and by comparison with the noise power spectra, we find $\kappa = 0.19$ to be the best value for the CMM.

We summarise the results of the calculation using these parameters in Fig. 5. In Fig 5(a), we show the permittivity, permeability and refractive index spectra, noting the frequency shift in both the permittivity and permeability between the CMM and the wires or rings due to the coupling described above. This leads to the negative refractive index region lying around 4.3 GHz, whereas the SRR resonance is at about 4.6 GHz. In Fig. 5(b), the calculated spectra for the transmission and emittance are compared with the measured S_{21} and noise power spectra. The main peak in the spectra for the SRRs alone is well described by the model; however, there is a low frequency tail to the noise spectrum, which is not reproduced. The wire spectra are not so well reproduced either: the measured transmission spectrum rises and the noise spectrum falls above 4.5 GHz, whereas the model shows a flat response. For the CMM, the noise peak and its high frequency tail are correctly obtained, but the calculations show a strong minimum in S_{21} at 4.3 GHz which is not present in the measured data, and the low frequency tail of the noise spectrum is not reproduced. Nevertheless, for such a simple model, the overall agreement obtained is reasonably good.

IV. DISCUSSION

As described above, the metamaterial that we used in this work was based on the original SRR material from Marconi, which provided a very convenient resonant frequency of 4.5 GHz. A more fundamental reason for choosing this material was its performance. It is a very dense material, with a unit cell spacing of 5.5 mm and an outer ring diameter of 5.0 mm: this is not typical for modern designs, which tend to be more dilute.[42] It is, however, well-suited to the present study because its high magnetic density means it is an intrinsically lossy material with a large μ'', and hence a large magnetic noise contribution: ideal for the present study. Furthermore, it was straightforward to design a fine wire structure with the required performance, which matched the unit cell size of the SRR material. We checked the performance of both the component parts and the CMM using HFSS, and this confirmed that there would be a negative index region in the neighbourhood of 4.5 GHz.

Ideally, we would have retrieved the permittivity and permeability spectra from S-parameter measurements, but this was not possible for two fundamental reasons: the demountable waveguide was not perfectly reproducible, so the calibrations were insufficiently robust, and the samples could not fill the waveguide completely. We therefore obtained data for various parameters in (6) and (7) in a piecemeal fashion. The resonant frequency of the rings was obtained by direct measurement, as were the plasma frequencies for the wires, both in the pure wire medium and the CMM. By using CRRs in combination with the wires, we have shown that there is indeed a negative index (or double negative) region above the SRR resonance. However, we have had to treat the damping terms in (6), (7) as unknown parameters, estimating them from the combination of the S-parameter and noise measurements. Being determined from the same data as the noise spectra means that the model parameters are a consistent practical set, rather than a theoretical estimate.

We used the switched source method to carry out the noise measurements because the signal from a passive measurement (as used in Ref. 38) was too close to the noise floor of our instrumentation. The advantage of the switched method is that one can extract both the transmission (or gain) of a sample, as well as its noise spectrum. There was substantial interference in the spectra, arising from the mismatched feed–waveguide transitions, and also from the sample faces themselves, but it was not possible to de-embed the data using calibration. We, therefore, placed the sample close to the input feed, so that there was effectively only one interference frequency, and used numerical filtering to de-embed the data. This is a robust approach, as the filter parameters could be reliably established from the empty guide transmission (S_{21}) spectra and were subsequently applied to both the sample S_{21} spectra and the noise spectra

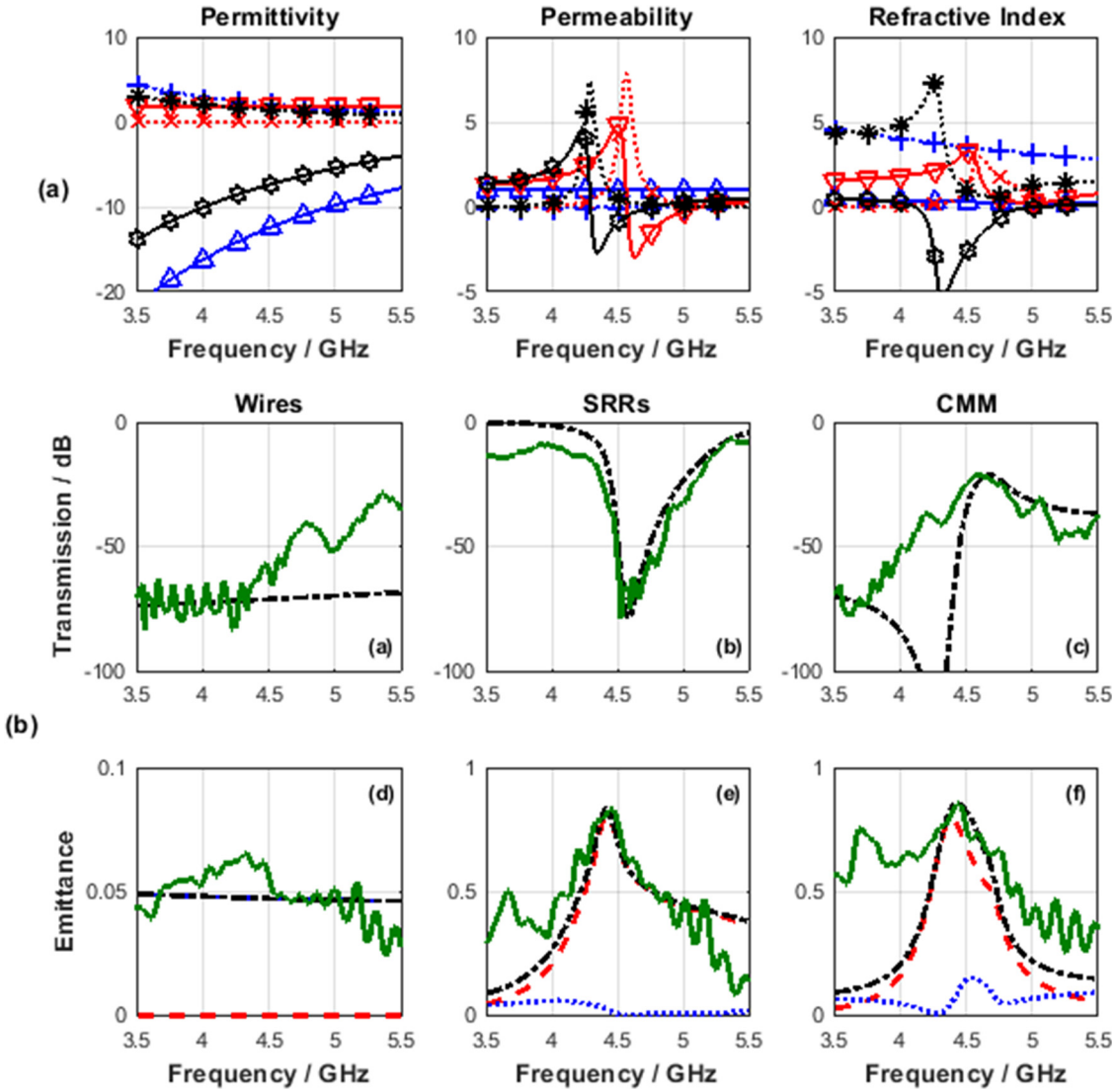

FIG. 5. The results of the transmission line model calculation. (a) The permittivity, permeability, and refractive index spectra of the 6-cell samples with parameters $f_0 = 4.68$ GHz, $F = 0.23$, $Q_0 = 35$, $\gamma_e = 0.15$, with $f_p = 12.5$ GHz for the wires alone, and 8.5 GHz for the CMM. The magneto-electric coupling parameter is $\kappa = 0.05$ for the SRRs alone and 0.19 in the CMM. Full lines show real parts for wires (blue △), rings (red ▽) and CMM (black ☆); dotted lines show imaginary parts for wires (blue +), rings (red x) and CMM (black *). (b) (a)–(c) Comparison of the measured and modelled transmission spectra; (d)–(f) Comparison of measured noise power with calculated emittance for (left to right) wires, rings and CMM. Green full lines show measured data, black chain lines are calculated values, with red dashed lines depicting the magnetic contribution and blue dotted lines the electric contribution to the noise power.

without modification. The transmission spectra thus obtained compare well with the S_{21} measurements.

From the system's point-of-view, it is often the noise figure, rather than the raw noise power that is of interest to developers. This measures the reduction in the signal-to-noise ratio that occurs when an element is included in the system and is a function of both the noise power and the transmission. Our data for the CMM [Figs. 2(f) and 3(f)] show that the incremental loss and the noise figure introduced by the metamaterial are both approximately 4.2 dB/unit cell, confirming that this is a very lossy, and hence noisy, medium.

We turn now to the modelling approaches. In our previous work,[38,39] we adopted a microscopic model based on a circuit theory. This has been extended[33] to describe metamaterials, using LC circuit elements for the SRRs and shunt inductors for the wires, incorporated into a transmission line model for free space. Although it is feasible to extend this model to 2-D and 3-D samples, it becomes numerically very cumbersome; so, in the present analysis, we have used the 1-D model developed by Ref. 33 who showed how the circuit approach could be reconciled with the macroscopic effective medium description of a metamaterial. This has allowed us to calculate the transmission and noise spectra based on effective medium parameters for the metamaterial samples.

What are the implications of these results for the application of metamaterials in practical systems? The key point arising from these data is that the magnetic noise is substantially larger than the dielectric noise. This is not surprising because the SRR is a resonant system and inevitably has a large χ'' close to the region where χ' is negative, whereas the susceptibility of the continuous wires is not resonantly enhanced, so the imaginary part remains small. Thus, in a practical system, we must concentrate on reducing the loss and noise in the SRRs. Using a low-loss board, the seminal work by Parazzoli *et al.*[6,23,24] achieved damping parameters

approximately an order of magnitude smaller than those found here; then, the noise is almost entirely due to the magnetic sub-system and is concentrated closely near the resonant frequency. Of course, in this region, the noise is large, but away from the immediate vicinity of the resonance, in what would be the useful working regime of a negative index device, the noise becomes quite small. Furthermore, since the transmission is also enhanced by the lower loss, the noise figure of such a material would be significantly lower than that found here; we would expect the noise figure for Parazzoli's material to be approximately 0.1 dB/unit cell. It is possible that this could lead to an acceptable performance for a microwave device, provided that it is only a few unit cells thick and can perform a function, like that of the MI cable,[15] that cannot be achieved with conventional materials.

V. CONCLUSIONS

We have measured and modelled the noise generated by a negative index (or double negative) metamaterial comprising split ring resonators and fine wires as the magnetic and dielectric components, respectively. The noise spectrum has contributions from both components, i.e. there is magnetic noise as well as more conventional electrical noise. We have also investigated the noise spectra of the two components independently and modelled these results. As expected, the magnetic noise is concentrated in the region of the resonant frequency of the SRRs (4.5 GHz) in both the SRR material and the CMM material. The electrical noise is spread over the entire spectrum, but with a broad peak showing at about 4.1 GHz in the wire material alone.

We have modelled the noise spectra using a one-dimensional circuit model, using the permittivity and permeability parameters of the materials as inputs to the noise model. In the circuit model, we represent the elements of the material by discrete capacitors, inductors and resistors, and sum the noise arising from the resistive elements to obtain the total noise. This approach has been successfully used for RF metamaterials, and was equally successful here, with good agreement achieved with the measured results.

The materials that we have investigated were deliberately made lossy, so that the noise would be measurable. In more practical materials, with lower loss components, the noise is still present, and our models show that the overall noise is dominated by the magnetic contribution from the resonant SRRs, whereas the dielectric noise is quite small. In a low-loss SRR material, the resonance is narrow, so the noise is confined close to the resonant frequency, and it may be possible to obtain useable performance at frequencies removed from the resonance of the SRRs. Nevertheless, because the magnetic noise dominates, practical applications are likely to be limited to functions that cannot be otherwise achieved.

ACKNOWLEDGMENTS

Support from the Leverhulme Trust through their award "Metamaterials and the Control of Electromagnetic Fields" is gratefully acknowledged.

[1]J. B. Pendry *et al.*, "Extremely low frequency plasmons in metallic mesostructures," Phys. Rev. Lett. **76**(25), 4773–4776 (1996).
[2]J. B. Pendry *et al.*, "Magnetism from conductors and enhanced nonlinear phenomena," IEEE Trans. Microwave Theory Tech. **47**(11), 2075–2084 (1999).
[3]D. R. Smith and J. B. Pendry, "Homogenization of metamaterials by field averaging (invited paper)," J. Opt. Soc. Am. B **23**(3), 391–403 (2006).
[4]D. R. Smith *et al.*, "Composite medium with simultaneously negative permeability and permittivity," Phys. Rev. Lett. **84**(18), 4184–4187 (2000).
[5]R. A. Shelby, D. R. Smith, and S. Schultz, "Experimental verification of a negative index of refraction," Science **292**(5514), 77–79 (2001).
[6]C. G. Parazzoli *et al.*, "Experimental verification and simulation of negative index of refraction using Snell's law," Phys. Rev. Lett. **90**(10), 107401 (2003).
[7]D. R. Smith, J. B. Pendry, and M. C. K. Wiltshire, "Metamaterials and negative refractive index," Science **305**(5685), 788–792 (2004).
[8]J. B. Pendry, "Negative refraction makes a perfect lens," Phys. Rev. Lett. **85**(18), 3966–3969 (2000).
[9]J. B. Pendry, D. Schurig, and D. R. Smith, "Controlling electromagnetic fields," Science **312**(5781), 1780–1782 (2006).
[10]D. Schurig *et al.*, "Metamaterial electromagnetic cloak at microwave frequencies," Science **314**(5801), 977–980 (2006).
[11]M. C. K. Wiltshire *et al.*, "Microstructured magnetic materials for RF flux guides in magnetic resonance imaging," Science **291**(5505), 849–851 (2001).
[12]V. C. Behr, A. Haase, and P. M. Jakob, "RF flux guides for excitation and reception in ^{31}P spectroscopic and imaging experiments at 2 Tesla," Concepts Magn. Reson., Part B **23B**(1), 44–49 (2004).
[13]R. R. A. Syms *et al.*, "Magnetic resonance imaging using linear magneto-inductive waveguides," J. Appl. Phys. **112**(11), 114911 (2012).
[14]R. R. A. Syms *et al.*, "Magneto-Inductive catheter receiver for magnetic resonance imaging," IEEE Trans. Biomed. Eng. **60**(9), 2421–2431 (2013).
[15]E. M. Kardoulaki *et al.*, "SNR in MI catheter receivers for MRI," IEEE Sens. J. **16**(6), 1700–1707 (2016).
[16]S. J. Lim, C. Caloz, and T. Itoh, "Metamaterial-based electronically controlled transmission-line structure as a novel leaky-wave antenna with tunable radiation angle and beamwidth," IEEE Trans. Microwave Theory Tech. **52**(12), 2678–2690 (2004).
[17]M. C. Johnson *et al.*, "Sidelobe canceling for reconfigurable holographic metamaterial antenna," IEEE Trans. Antennas Propag. **63**(4), 1881–1886 (2015).
[18]W. N. Hardy and L. A. Whitehead, "Split-Ring resonator for use in magnetic-resonance from 200-2000 MHz," Rev. Sci. Instrum. **52**(2), 213–216 (1981).
[19]M. C. K. Wiltshire, "Radio frequency (RF) metamaterials," Phys. Status Solidi B **244**(4), 1227–1236 (2007).
[20]R. R. A. Syms *et al.*, "Thin-film magneto-inductive cables," J. Phys. D: Appl. Phys. **43**(5), 055102 (2010).
[21]M. C. K. Wiltshire *et al.*, "Dispersion characteristics of magneto-inductive waves: Comparison between theory and experiment," Electron. Lett. **39**(2), 215–217 (2003).
[22]G. Dolling *et al.*, "Low-loss negative-index metamaterial at telecommunication wavelengths," Opt. Lett. **31**(12), 1800–1802 (2006).
[23]R. B. Greegor *et al.*, "Origin of dissipative losses in negative index of refraction materials," Appl. Phys. Lett. **82**(14), 2356–2358 (2003).
[24]C. G. Parazzoli *et al.*, "Performance of a negative index of refraction lens," Appl. Phys. Lett. **84**(17), 3232–3234 (2004).
[25]J. B. Johnson, "Thermal agitation of electricity in conductors," Phys. Rev. **32**(1), 97–109 (1928).
[26]H. Nyquist, "Thermal agitation of electric charge in conductors," Phys. Rev. **32**(1), 110–113 (1928).
[27]H. B. Callen and T. A. Welton, "Irreversibility and generalized Noise," Phys. Rev. **83**(1), 34–40 (1951).
[28]H. B. Callen and R. F. Greene, "On a theorem of irreversible thermodynamics," Phys. Rev. **86**(5), 702–710 (1952).
[29]R. Kubo, "The fluctuation-dissipation theorem," Rep. Prog. Phys. **29**(1), 255 (1966).
[30]R. Kubo and K. Tomita, "A general theory of magnetic resonance absorption," J. Phys. Soc. Jpn. **9**, 888–919 (1954).
[31]S. M. Rytov, *Theory of Electric Fluctuations and Thermal Radiation* (Academy of Sciences, Moscow, 1953); Translated by Air Force Cambridge Research Center TR-59-162.
[32]D. X. Chen, E. Pardo, and A. Sanchez, "Demagnetizing factors of rectangular prisms and ellipsoids," IEEE Trans. Magn. **38**(4), 1742–1752 (2002).

[33]R. R. A. Syms, O. Sydoruk, and L. Solymar, "Noise in one-dimensional metamaterials supporting magnetoinductive lattice waves," Phys. Rev. B **87**(15), 155155 (2013).
[34]R. R. A. Syms, O. Sydoruk, and L. Solymar, "Transmission-line model of noisy electromagnetic media," IEEE Trans. Microwave Theory Tech. **61**(1), 14–22 (2013).
[35]J. R. Pierce, "Physical sources of noise," Proc. IRE **44**(5), 601–608 (1956).
[36]E. Shamonina *et al*., "Magnetoinductive waves in one, two, and three dimensions," J. Appl. Phys. **92**(10), 6252–6261 (2002).
[37]M. Beruete *et al*., "Electroinductive waves in chains of complementary metamaterial elements," Appl. Phys. Lett. **88**(8), 083503 (2006).
[38]M. C. K. Wiltshire and R. R. A. Syms, "Measuring trapped noise in metamaterials," J. Appl. Phys. **115**(8), 084905 (2014).
[39]M. C. K. Wiltshire and R. R. A. Syms, "Noise performance of magnetoinductive cables," J. Appl. Phys. **116**(3), 034503 (2014).
[40]K. Aydin *et al*., "Experimental observation of true left-handed transmission peaks in metamaterials," Opt. Lett. **29**(22), 2623–2625 (2004).
[41]C. M. Soukoulis *et al*., "The science of negative index materials," J. Phys.-Condens. Matter **20**(30), 304217 (2008).
[42]D. R. Smith *et al*., "Design and measurement of anisotropic metamaterials that exhibit negative refraction," IEICE Trans. Electron. **E87C**(3), 359–370 (2004).
[43]N. Katsarakis *et al*., "Left- and right-handed transmission peaks near the magnetic resonance frequency in composite metamaterials," Phys. Rev. B **70**(20), 201101 (2004).
[44]A. M. Nicolson and G. F. Ross, "Measurement of intrinsic properties of materials by time-domain techniques," IEEE Trans. Instrum. Meas. **19**(4), 377–382 (1970).
[45]W. B. Weir, "Automatic measurement of complex dielectric constant and permeability at microwave frequencies," Proc. IEEE **62**(1), 33–36 (1974).
[46]D. R. Smith *et al*., "Determination of effective permittivity and permeability of metamaterials from reflection and transmission coefficients," Phys. Rev. B **65**(19), 195104 (2002).
[47]G. F. Engen and C. A. Hoer, "Thru-Reflect-Line - Improved technique for calibrating the dual 6-port automatic network analyzer," IEEE Trans. Microwave Theory Tech. **27**(12), 987–993 (1979).
[48]Y. Liu *et al*., "Measurements of planar microwave circuits using an improved TRL calibration method," Prog. Electromagn. Res.-Pier **109**, 263–278 (2010).
[49]H. T. Friis, "Noise figures of radio receivers," Proc. IRE **32**(7), 419–422 (1944).
[50]Continental Compliance Ltd., 27 Weelsby Way, Hessle, East Yorkshire, HU13 0JN, UK.
[51]HD Communications Corp., 2180 Fifth Avenue, Unit 4, Ronkonkoma, NY 11779, USA.